Radiation Response of Perfluorinated Polymer Optical Fibers (CYTOP) to Low Doses of X-Rays, Protons, and Neutrons

Olugbenga Jeremiah Olusoji, *Member, IEEE*, Crystal Penner, *Member, IEEE*, Camille Bélanger-Champagne, *Member, IEEE*, Vince Strgar, Eva Kasanda, Cornelia Hoehr, and Sinead O'Keeffe, *Member, IEEE*

***Abstract*—The response of perfluorinated polymer fibers (PF-POFs) in X-ray, proton, and neutron irradiation was investigated for their potential application in clinical environments. Radiation-induced attenuation (RIA) in PF-POF increases linearly with dose and PF-POF was found to be highly sensitive to all the sources of radiation used. A sensitivity of 0.050 ± 0.003, 0.089 ± 0.005, and 0.065 ± 0.003 dB/m/Gy was recorded for 6 MV X-rays, 63 MeV protons, and 400 MeV neutrons, respectively, at a wavelength of 510 nm at room temperature. The PF-POF fibers also exhibit energy dependence—a useful feature in characterizing the depth dose in a proton beam. The high sensitivity of the fiber enables the development of distributed sensing in oncology and can be combined with other solid-state detectors in monitoring radiation dose in mixed radiation environments.**

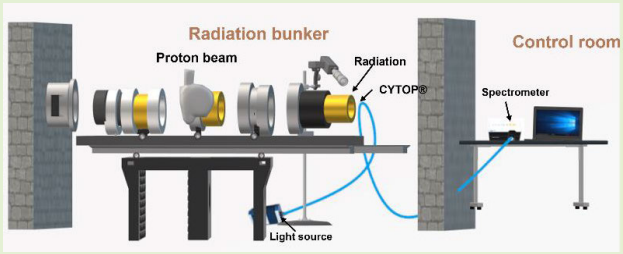

***Index Terms*—Cyclic transparent optical polymer (CYTOP), dosimetry, neutron, optical fiber, optical sensor, proton therapy, radiation-induced attenuation (RIA), X-ray.**

I. Introduction

RADIOTHERAPY can be delivered via X-ray, proton, or neutron beams. The past years have led to advancements in radiation delivery to cancerous cells and tumors while avoiding neighboring sensitive organs and healthy tissue. Some of these techniques involve the modulation of the intensity of the radiation and/or the scanning of the beam across the tumor to map out a 3-D treatment pattern. The modification of the beam involves the division of the beam into small fields and their superposition to fit the treatment planning system and shape of the tumor. These complex techniques have driven the demand for improvements in dosimeters for accurate characterization of the beam intensity, shape, and size [1], as the dosimeter is faced with steep dose gradients, partial occlusion of radiation sources, and absence of electronic equilibrium due to the small fields [2].

The gold standard for dosimeters in X-ray irradiation is the ionization chamber which is typically bulky in size and lacks physical flexibility. For resolving small fields, the large size of the ionization chamber leads to an underestimation of the dose maximum and an overestimation of the penumbral region as a result of the larger volume averaging effect [3]; these sensors are also only capable of interrogating one point at a time.

Optical fibers possess several characteristics that give them advantages in measuring small radiation field sizes, and they have been used in various dosimetry applications due to their flexibility, robustness in radiation environment, immunity to electromagnetic interference, superior spatial resolution, near water-equivalence in organic fibers, and proven applications

Manuscript received 27 July 2023; revised 18 September 2023; accepted 22 September 2023. Date of publication 5 October 2023; date of current version 14 November 2023. This work was supported in part by the Royal Society and Science Foundation Ireland (SFI) through the Royal Society—SFI University Research Fellowship under Grant UF150618, in part by the Royal Society—SFI Enhancement Award under Grant RGF/EA/180166, and in part by the TRIUMF receives federal funding via a contribution agreement with the National Research Council of Canada. The associate editor coordinating the review of this article and approving it for publication was Dr. Xuehao Hu. *(Corresponding author: Olugbenga Jeremiah Olusoji.)*

Olugbenga Jeremiah Olusoji and Sinead O'Keeffe are with the Optical Fiber Sensors Research Center, University of Limerick, V94 T9PX Limerick, Ireland (e-mail: olugbenga.olusoji@ul.ie; sinead.okeeffe@ul.ie).

Crystal Penner, Camille Bélanger-Champagne, and Cornelia Hoehr are with TRIUMF, Vancouver, BC V6T 2A3, Canada (e-mail: cpenner@triumf.ca; cbchampagne@triumf.ca; choehr@triumf.ca).

Vince Strgar is with BC Cancer, Vancouver, BC V5Z 4E6, Canada (e-mail: vstrgar@bccancer.bc.ca).

Eva Kasanda is with the Albert Einstein Center for Fundamental Physics (AEC), Laboratory for High Energy Physics (LHEP), University of Bern, 3012 Bern, Switzerland (e-mail: eva.kasanda@unibe.ch).

Digital Object Identifier 10.1109/JSEN.2023.3320874

in real-time in vivo dosimetry [1], [2], [4], [5]. Optical fiber sensors have not only been used for the characterization of proton and photon beams, they have also been used for brachytherapy applications [6], [7], [8].

The majority of the sensors developed with optical fibers are based on the attachment of organic or inorganic scintillators at the tip of optical fibers, and the radiation-induced luminescence (RIL) in the scintillator is measured. The various geometries of attaching the scintillators include the recoating of a stripped section of the cladding with a scintillator, the filling of a drilled hole at the tip with scintillating powder, and epoxy and the formation of a helical shape of the scintillator on the tip of the fiber. The scintillator couples the light output into the fiber which mostly acts as a transport medium for the generated light [9], [10]. This approach is limited to the single point of the scintillator or at most a small number of sensing points due to restrictions from the types of scintillating material used and the design and dimensions of the sensor [11], [12]. Scintillators are also prone to quenching in regions of high linear energy transfer (LET), as well as to induced Cherenkov light contamination, and corrections for these shortcomings must be considered.

An alternative approach is to use the inherent reaction of the fiber itself during material interaction with radiation. The effects on the material making up the fiber can either lead to color center formation, radiation-induced attenuation (RIA), or radiation-induced emission (RIE), and the resulting intensities of these mechanisms depend on the constituent material of the fiber. In sensing applications, the RIA in the fiber can be used to develop a spatially distributed sensor. The magnitude of the RIA is dependent on several aspects and can be tailored to the application via several choices: type of fiber including core and cladding composition [13], [14], drawing condition [15], impurities [16], and fiber stoichiometry [17]; irradiation conditions including nature of particle [18], dose (fluence) [19] temperature [20], and dose rate [21]; and fiber condition including preirradiation [22], injected power [23], and preloading conditions [24], [25].

The use of polymer fibers has been pursued in clinical applications due to their water-equivalent nature, their biocompatibility in tissue, their transparency in imaging systems, and being less brittle than glass fibers [26]. Several reports have shown the response of perfluorinated fiber to gamma rays [26], X-rays [27], and protons [28]. The radiation sources used in clinical applications often include a small proportion of neutrons [29]. Perfluorinated polymer fiber (PF-POF) was used for the test because they have excellent transmission in the visible and infrared wavelength in comparison to polycarbonate or polymethyl methacrylate (PMMA)-based POF. They can be integrated as quasi-distributed sensors or distributed sensors with commercially available interrogators and distributed systems. The goal of this study is to characterize the energy dependence and dose-rate dependence of the PF-POF for potential use in dosimetry applications in photon, proton, and neutron radiation fields.

This is the first study on the comparison between the interaction of protons, neutrons, and X-rays on perfluorinated polymer optical fiber.

II. Materials and Methods

A. Materials

The optical fiber used for the sensor is a commercially available multimode GigaPOF-50SR polymer fiber produced by CHROMIS (USA) [33]: it is a perfluorinated fiber with a cyclic transparent optical polymer (CYTOP) core material with a diameter of 50 μm and a Xylex (a blend of polyester and polycarbonate) cladding with a diameter of 490 μm. The fiber is prepared by the co-extrusion process where the CYTOP dopant is diffused with thermal polymerization to form the graded index profile from the dopant in the extruder [34]. Two meters of the fiber were inserted into a black jacket BK-090 [35] from Thorlabs to block out ambient light, terminated at both ends with subminiature version A (SMA)-905 connectors, and the ends polished with 5 μm and then 1 μm lapping paper.

One end of the CYTOP fiber was coupled to a light source and the other end to a 15 m length of a 1000 μm core PMMA transport fiber via an SMA-SMA mating sleeve filled with a refractive index matching liquid. The other end of the PMMA was connected to an SM442-URN010-USB spectrometer (Spectral Products) to monitor the intensity change to measure the RIA. The spectrometer was connected to a computer for data taking and analysis. The dark spectrum, taken before switching on the light source, was subtracted from the measured spectrum to correct for background signal. The long lengths of PMMA fiber ensured the spectrometer and the PC remained in the control area, away from the radiation. The general setup of the experiment is shown in Fig. 1. The light source used for the X-ray and neutron measurements was a HL-2000-LL (Ocean Insight) Tungsten-Halogen lamp, while the light source used for proton irradiation was a LS-1 (Ocean Insight) Tungsten-Halogen lamp. The light source was shielded from background radiation in the radiation room. The stability of the probing light was ensured before the start of the experiment.

B. Irradiation Experiments

1) Proton Irradiation: Proton irradiations were conducted at the Proton Therapy Research Center (PTRC), a previous clinical facility at TRIUMF, Vancouver, Canada, [30]. A 70 MeV beam was extracted from the cyclotron. The energy at the experimental position, after traversing beam delivery and monitoring devices is 63 MeV and can be further degraded to 35, 20, and 9 MeV with an extracted beam current ranging from 3 to 9 nA. The beam was collimated to a size of 5 by 5 cm square, similar to the setup described by Olusoji et al. [28]. The radiation treatment room is temperature controlled.

The PF-POF was attached to the upstream side of a PMMA support plate, with a 12 cm length of the fiber being in the irradiation field [see Fig. 2(a)].

The delivered dose was monitored during the irradiation with an in-line ionization chamber. The standard unit of dose measurement is monitor counts (MCs) and the conversion factor from MC to fluence or dose depends on the proton energy. An estimation of the accumulated dose at the specific proton energies was evaluated by SRIM [31] and Geant4 [32] simulations as shown in Table I. The in-line ionization

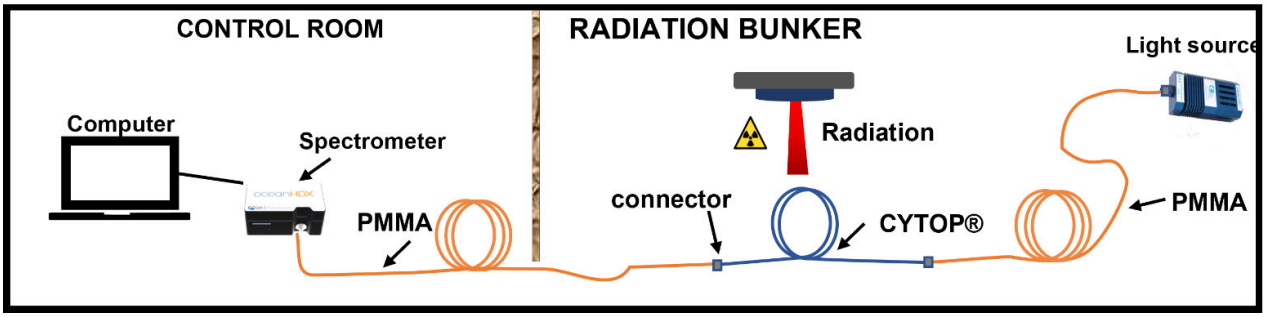

Fig. 1. General setup of the experiment.

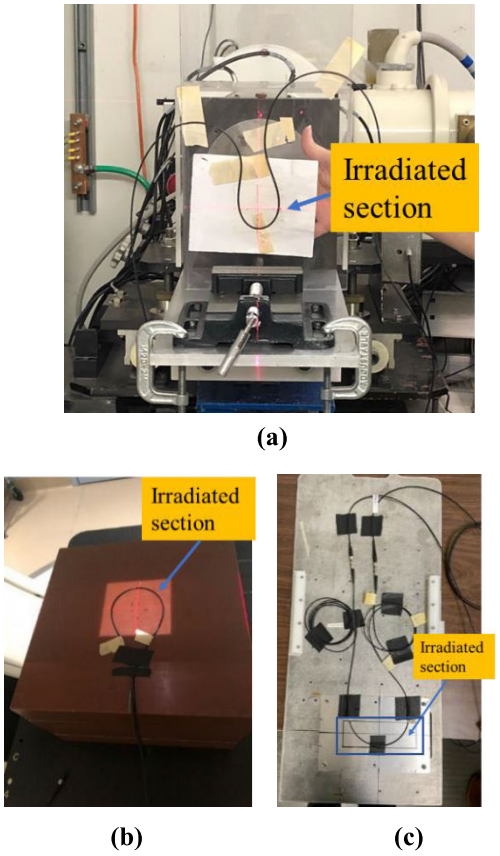

Fig. 2. (a) Setup of the fiber on the PMMA support plate for the proton experiments. (b) Setup of the fiber on X-ray couch on top of 20 cm solid water backscatter. (c) Setup of the fiber on the aluminum support plate for TNF.

TABLE I
SRIM AND GEANT4 ESTIMATION OF THE MC TO Gy CONVERSION AT DIFFERENT ENERGIES

Energy	9 MeV	20 MeV	35 MeV	63 MeV
cGy/ 10000 MC	88	92	89	108

chamber was calibrated against an Exradin T1 ionization chamber for which the absolute dose calibration is known.

Continuous acquisition of the spectrum with the spectrometer was initiated as the proton shutter was opened and the fiber was irradiated. The fiber was initially irradiated at a beam energy of 63 MeV at a current of 6 nA to a total of 80.8 Gy. Subsequent measurements were taken during irradiations of the fiber at different energies and dose rates. The energies were degraded with an in-beamline energy degrader called a range shifter as described by Blackmore [30].

2) X-Ray Irradiation: X-ray measurements were conducted at BC Cancer (Vancouver, Canada), an active clinical facility. The fiber was irradiated with a Vero linear accelerator. Tests were conducted using a flattened, filtered beam with energy spectra peaking at 6 MV, a beam size of 10 × 10 cm, dose build-up (water equivalent material on top of the fiber) of 1.5 cm, and backscatter (water equivalent material below the fiber) of 20 cm. The standard unit of measurement is monitor unit (MU). Two dose rates were tested: 3 and 5 Gy/min. The radiation treatment room is temperature controlled. A 22-cm length of the perfluorinated fiber was fastened to a solid water slab and coiled fully within the beam limits as shown in Fig. 2(b).

3) Neutron Irradiation: For RIA testing in neutrons, 17.5 cm of CYTOP fiber was inserted into the TRIUMF neutron facility (TNF) neutron field. TNF neutrons are created by spallation reaction when high energy protons (typically around 400 MeV depending on upstream beamline conditions) are stopped in a water moderator containing aluminum plates [33]. The neutron field is accessible by a 5 m-long vertical shaft where an aluminum board, which is fit to a pulley mechanism, is manually lowered until the plate reaches the bottom of the shaft. The board is marked with the neutron irradiation area and the length of fiber to be irradiated was taped to the board so as to ensure the maximum length would be irradiated as seen in Fig. 2(c). For the neutron irradiation, the plate with the fiber attached was lowered into the neutron field. After irradiation, the plate was pulled up and out of the field. The average neutron flux was 8.2×10^6 n/(cm^2 s) with a dose rate of 3.18×10^{-4} Gy/s for neutrons > 0.1 MeV.

C. Data Analysis

The RIA was extrapolated from the Beer-Lambert law of absorption by considering the changes in the intensity of the transmitted spectrum over time using

$$\mathrm{RIA_{dB}} = -\frac{10}{L_0} \log \left\{ \frac{I_t(\lambda, t)}{I_0(\lambda)} \right\} \quad (1)$$

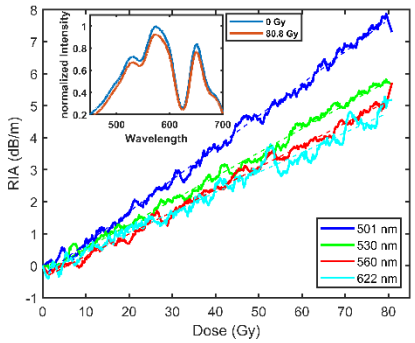

Fig. 3. RIA for specific doses at proton energy of 63 MeV and extracted beam current of 6 nA. Inset: Spectrum of the normalized intensity before radiation and after 80.8 Gy of proton radiation at 63 MeV.

$$S = \frac{\Delta \mathrm{RIA}_{\mathrm{dB}}}{\Delta D_{\mathrm{Gy}}} \tag{2}$$

where L_0 is the length of the irradiated fiber, $I_t(\lambda, t)$ is the optical intensity measured continuously during the irradiation, $I_0(\lambda)$ is the intensity measured before the fiber was irradiated, $\mathrm{RIA}_{\mathrm{dB}}$ is the RIA in the fiber in dB, and S is the sensitivity of the fiber: a linear slope of the RIA with dose (ΔD_{Gy}). The evolution of the intensity with time was used to obtain the RIA for the dose in Gray (Gy). The spectrometer was run at a low integration time to obtain data with a high resolution of RIA as a function of dose.

III. Results

A. Proton Results

1) Dose-Response: The RIA caused by proton irradiation is shown in Fig. 3 for different wavelengths. The RIA is calculated from the intensity using (1). The fiber shows a strong response to proton radiation. The intensity of the transmitted light signal across all wavelengths decreases and therefore the RIA increases as the proton dose increases. The fiber response is linear in the dose and energy ranges included in the study. The slope of the RIA curve with dose varies for the different wavelengths. Overall, RIA increases more as the wavelength tends toward the UV with a sharp increase in the RIA as the wavelength goes below 530 nm. The sensitivity at other selected wavelengths is shown in Table II.

2) Energy Dependence: To determine the dependence of the fiber response on the energy of the protons, in addition to the undegraded 63 MeV, the proton beam was degraded to energies of 9, 20, and 35 MeV with the in-beamline range shifter, and the fiber was irradiated at a constant extracted current of 6 nA. Wavelengths with high signal-to-noise ratios were selected to observe this dependence. The fiber was irradiated to an average total MC of 750 000 MC, which corresponds to an estimated total dose for the different proton energies of 80.8, 67, 68.8, and 66 Gy for 63, 35, 20, and 9 MeV, respectively. The fiber sensitivity shows a dependence on the energy of the proton beam across all wavelengths, that is, the slope of the RIA with dose increases as the energy of the beam increases (see Table II and Fig. 4).

The sensitivity of the fiber as a function of interrogated wavelengths is shown in Fig. 4(a) and as a function of proton energy for selected wavelength in Fig. 4(b). The CYTOP fiber exhibits higher sensitivity for higher proton energies. The shown sensitivity is limited to wavelengths between 450 and 700 nm due to inherent attenuation in the PMMA extension fiber leading to large uncertainties from the low signal-to-noise ratio.

TABLE II
Sensitivity at Different Proton Energies With Estimated Error From Fiber Placement in the Beam

Wavelength (nm)	Sensitivity (dB/m/Gy) × 10^{-2}			
	9 MeV	20 MeV	35 MeV	63 MeV
450	7.00±0.4	8.91±0.4	10.37±0.5	15.36±0.8
480	9.54±0.5	10.83±0.5	12.89±0.7	15.08±0.8
529	6.35±0.3	7.44±0.4	7.83±0.4	7.67±0.4
555	5.22±0.3	6.33±0.3	6.74±0.3	6.92±0.4
577	5.42±0.3	6.24±0.3	6.99±0.4	7.15±0.4
653	5.79±0.3	7.09±0.4	7.83±0.4	8.57±0.4

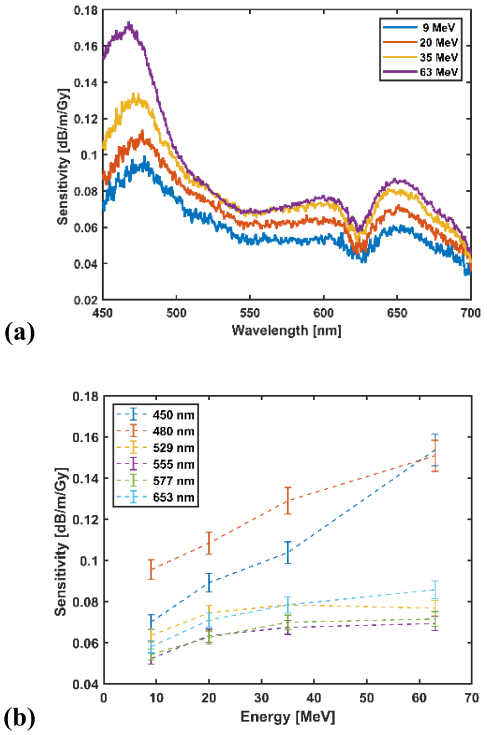

Fig. 4. (a) Sensitivity dependence on proton energy for all wavelengths. (b) Sensitivity dependence on proton energy for selected wavelengths.

3) Dose Rate Dependence: The dependence on the proton dose rate of the sensitivity of the PF-POF fiber was also explored: the fiber was irradiated with beam currents of 3, 6, and 9 nA at a constant proton energy of 63 MeV. The sensitivity of the fiber across all the wavelengths for each dose rate is shown in Fig. 5(a), while the sensitivity at selected

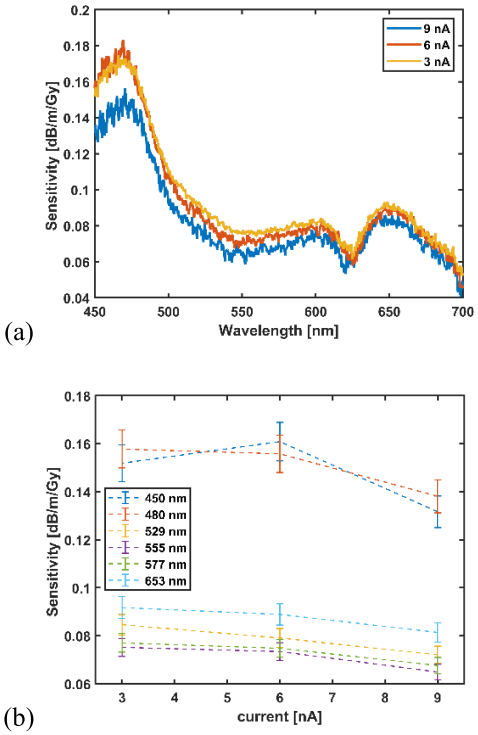

Fig. 5. (a) Sensitivity dependence on proton dose rate for all wavelengths. (b) Sensitivity dependence on proton dose rate for selected wavelengths.

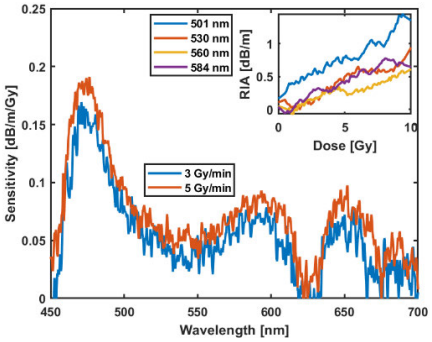

Fig. 6. Sensitivity to X-ray irradiation as a function of wavelengths for dose rates of 3 and 5 Gy/min. Inset: RIA as a function of X-ray dose at selected wavelengths at a dose rate of 5 Gy/min.

wavelengths is shown in Fig. 5(b). At selected wavelengths with a high signal-to-noise ratio, a clear distinction cannot be associated with the change in the dose rate: there are wavelengths where the difference in the dose rate was minimal (620–650 nm) and there are wavelengths where the influence of the dose rate is significant (450–600 nm). The relative standard deviation is highest at 6 nA for all selected wavelengths.

B. X-Ray Results

To test the response to X-rays, the fiber was irradiated to a total of 1000 MU (≡10 Gy at the described conditions) with a field size of 10 × 10 cm and a source-to-surface distance (SSD) of 100 cm. Equation (1) was used for the analysis of the result as in the proton beam experiment. The resulting sensitivity is shown in Fig. 6 as a function of wavelengths.

TABLE III
SENSITIVITY OF PF-POF TO 6 MV X-RAYS AT A DOSE RATE OF 500 MU/min, 63 MeV PROTONS AT 6 nA AND NEUTRONS AT SELECTED WAVELENGTHS WITH ERROR FROM FIBER PLACEMENT IN THE BEAM

Wavelength (nm)	Sensitivity (dB/m/Gy) $*10^{-2}$		
	Xray	Proton	TNF
510	5.04 ± 0.3	8.91 ± 0.5	6.53 ± 0.3
530	4.49 ± 0.2	7.78 ± 0.4	5.82 ± 0.3
560	4.88 ± 0.2	6.92 ± 0.4	5.42 ± 0.3
584	7.20 ± 0.4	7.41 ± 0.4	5.46 ± 0.3

The light intensity measured by the spectrometer reduces at all wavelengths as the dose accumulates. The RIA increases linearly as the dose increases across all wavelengths when irradiated to a total dose of 10 Gy (Fig. 6: inset). The PF-POF fiber is significantly more sensitive to X-ray radiation at wavelengths below 500 nm while showing a low and fairly stable sensitivity between 500 and 600 nm. The sensitivity values at selected wavelengths for 6 MV radiation at a dose rate of 5 Gy /min is shown in Table III. Overall, the PF-POF has higher sensitivity (across all wavelengths) for higher dose rates for X-ray with a mean difference of 20% between a wavelength of 500–600 nm.

C. Neutron Results

PF-POF response to neutron radiation was acquired using similar techniques to that for X-ray and proton radiation. The light spectrum was taken before the fiber was lowered into the irradiation chamber, where the fiber was exposed for 21 h to a total dose of approximately 21 Gy. The RIA as a function of neutron dose at selected wavelengths is shown in Fig. 7, while the sensitivity as a function of wavelengths is shown in Fig. 7 (inset). Overall, the RIA in the fiber increases as the neutron dose increases, but the slope of the RIA has two different regions: there is a lower sensitivity of the fiber for the first 5 Gy delivered, and a steeper increase of the RIA after that. The sensitivity curve for neutron irradiation is noisier than that of protons or X-rays and is noisiest at the wavelengths where the light source intensity is lowest [see Fig. 8(b)], worsening the signal-to-noise ratio. The sensitivity increases as the wavelengths tend toward the UV region. The recovery of the fiber in neutron cannot be measured because pulling the fiber out of the neutron hole distorts the transmission in the fiber.

D. Comparison Between Different Irradiations

The comparison of the sensitivity of the PF-POF fiber as a function of wavelengths to X-rays, protons, and neutrons is shown in Fig. 8. While overall, the sensitivities do follow the same behavior, there are significant difference between the magnitude of the sensitivity acquired for the different radiation

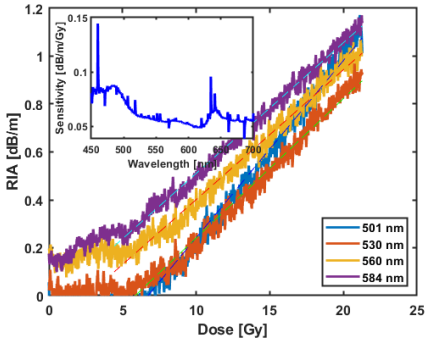

Fig. 7. RIA as a function of neutron dose at selected wavelengths. Inset: Sensitivity to neutron irradiation as a function of wavelengths.

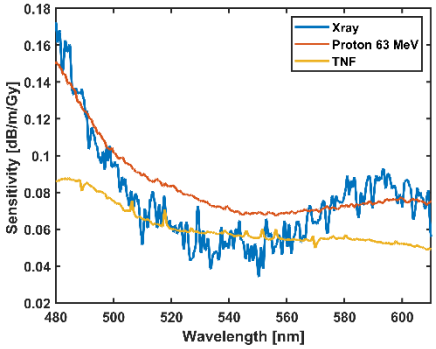

Fig. 8. Comparison between the sensitivity to neutron, X-ray, and proton radiation: neutron (flux 8.2 × 106 n/(cm^{2}s) dose rate of 3.18 × 10^{-4} Gy/s), X-ray (6 MV, 5 Gy/min), and proton (63 MeV, 6 nA).

types. It is worthy to note that there is a difference in the dose rate, energy, and experimental condition contributing to these differences. Further experiments will be conducted to prove the difference using similar radiation parameters.

IV. Discussion

The radiation response of PF-POF was studied to understand the interaction of protons, neutrons, and X-rays for a possible application as a sensing element in dosimetry. RIA is commonly used to identify the effect of radiation on optical fiber, i.e., the damage induced in the fiber from radiation [34]. In polymer fibers, the radiation source is expected to induce a chain scission process from the breakage of bonds within the polymer chain, which leads to a decrease in the molecular weight and the viscosity of the fiber and is characterized by an increase in the solubility of the polymer material. This effect is predominant in PMMA and PF-POF [35], [36].

The RIA in all studied fibers increases as the radiation dose increases for all the sources of radiation. The increase of the RIA is linear in both the X-ray and proton irradiation. For the neutron irradiation, the RIA initially displays only a very small increase, but after a dose of 5–10 Gy, a larger linear increase of RIA is observed, as shown in Fig. 7. This could be a result of the relatively low dose rate from the neutrons as compared to protons and X-rays, causing a delayed activation of the chain scission process in the fiber.

The RIA in the PF-POF varies with wavelength for all beam types. The fiber shows a strong sensitivity to all sources of radiation. The sensitivity of the fiber increases as it moves toward the UV region, as the absorption rate at each defect site, referred to as free radicals in polymers from chain scission, varies, as supported by electron paramagnetic resonance (EPR). EPR measurement on PF-POF by Stajanca et al. [26] in gamma-ray and Leal-Junior et al. [37] in gamma and electron radiation, suggests that the RIA observed from the chain scission process is a combination of the absorption of free radicals (unstable at room temperature) and the absorption of new compounds with an increased conjugated degree (stable at room temperature), which account for the stable RIA [26]. The depletion of these free radicals is reported by Olusoji et al. [28]: after the movement of a single fiber across the Bragg peak of a proton beam, wavelengths with an initial strong sensitivity (451 nm) at the entrance have a lower response at the Bragg peak, while wavelengths with a low response at the entrance show a strong sensitivity at the Bragg peak, an effect of the reduction of free radicals generated. The strong sensitivity observed from the different sources of radiation and the more permanent RIA after a partial recover at room temperature can also be linked to the formation of conjugated pairs.

The overall sensitivity to neutrons is lower in comparison to protons and X-rays. This could be a result of a lower interaction of the fiber with the neutrons or the low dose rate. The fiber exhibits energy dependence in protons, and a previous report by Olusoji et al. [27] shows an energy dependence in X-rays. The sensitivity of the fiber in protons increases as the energy increases, although the relative standard deviation at higher energies increases as well. Additional work with monoenergetic or quasi-monoenergetic neutron sources would be needed to determine if the fiber response also varies with neutron energy.

The energy dependence is useful for the characterization of the depth dose deposition of a proton beam, and a wavelength between 500 and 600 nm is recommended as the fast depletion at shorter wavelengths and fast saturation of the RIA as a result of the higher sensitivity give an underrepresentation of the spectrum of the Bragg peak. The low dependence of the fiber on the dose rate, especially in protons, makes the fiber useful for developing a dosimeter that is largely independent of the dose rate. PF-POF has a potential as a reusable sensor as Sporea et al. [38] reported a linear response of the fiber of up to 1.3 kGy of gamma irradiation at a wavelength of 642 and 713 nm. PF-POF has a fast partial recovery and recovery of 5% after 2 h at room temperature, with good reproducibility and repeatability [39]. A protective jacket is needed for its use as a sensing element as there a reported increases in the affinity for humidity from radiation damage [26].

Given the high sensitivity of the PF-POF, in comparison to undoped PMMA, and its dependence on radiation energy, an inexpensive LED light source can be used with an inexpensive detector to develop a low-cost dosimeter for application in clinical practice. The fiber can be integrated as a distributed sensor with widely available distributed systems such as optical time domain reflectometry (OTDR) and optical frequency domain reflectometry (OFDR) to monitor radiation in various sources of radiation, as in the

report by Di Francesca et al. [40], Toccafondo et al. [41], and Girard et al. [42] where a phosphorus-doped silica fiber was used to characterize the Bragg peak of a proton synchrotron, distributed monitoring of a mixed environment at "Cern High energy AcceleRator Mixed field facility (CHARM)," [41] and distributed neutron monitoring at TNF [42], respectively.

V. Conclusion

This study compares the response of perfluorinated polymer to different radiation sources (X-ray, proton, and neutron) at different energies and dose rates. This is the first study on the RIA effect of neutrons on these fibers. The RIA in the fiber at different dose rates and energies is linear with the accumulated dose at the wavelengths considered. In addition, the fiber shows an energy dependence to proton beam energy and a relatively low dose rate dependence on proton beams. The fiber is sensitive to all types of radiation used, making it applicable for sensing in different radiation types with the potential for integrating it for distributed measurement in a clinical setting. The difference in response to different radiation types may make it possible to distinguish the absorbed dose from different particles when combined with other sensors [43].

Acknowledgment

The authors would like to thank BC Cancer for their assistance and for the use of their linear accelerator.

References

[1] L. Beaulieu and S. Beddar, "Review of plastic and liquid scintillation dosimetry for photon, electron, and proton therapy," *Phys. Med. Biol.*, vol. 61, no. 20, pp. R305–R343, Oct. 2016.

[2] M. Gonod et al., "Miniaturized scintillator dosimeter for small field radiation therapy," *Phys. Med. Biol.*, vol. 66, no. 11, Jun. 2021, Art. no. 115016.

[3] A. Schönfeld, K. Mund, G. Yan, A. A. Schönfeld, H. K. Looe, and B. Poppe, "Corrections of photon beam profiles of small fields measured with ionization chambers using a three-layer neural network," *J. Appl. Clin. Med. Phys.*, vol. 22, no. 12, pp. 64–71, Dec. 2021.

[4] J.-C. Gagnon et al., "Dosimetric performance and array assessment of plastic scintillation detectors for stereotactic radiosurgery quality assurance," *Med. Phys.*, vol. 39, no. 1, pp. 429–436, Dec. 2011.

[5] C. Hoehr et al., "Novel Gd^{3+}-doped silica-based optical fiber material for dosimetry in proton therapy," *Sci. Rep.*, vol. 9, no. 1, pp. 4–11, Nov. 2019.

[6] P. Woulfe, S. O'Keeffe, and F. J. Sullivan, "EP-1800: Optical fibre luminescence sensor for real-time LDR brachytherapy dosimetry," *Radiotherapy Oncol.*, vol. 123, pp. S988–S989, May 2017.

[7] C. Hoehr et al., "Optical fibers for dosimetry in external beam therapy," in *Proc. Opt. Sensors Sens. Congr.*, 2020, Art. no. STu5D.2.

[8] S. Girard et al., "X-rays, γ-rays, and proton beam monitoring with multimode nitrogen-doped optical fiber," *IEEE Trans. Nucl. Sci.*, vol. 66, no. 1, pp. 306–311, Jan. 2019.

[9] J. Archer and E. Li, "Recent advances in photonic dosimeters for medical radiation therapy," *Frontiers Optoelectronics*, vol. 11, no. 1, pp. 23–29, Mar. 2018.

[10] C. Penner, C. Hoehr, S. O'Keeffe, P. Woulfe, and C. Duzenli, "Characterization of a terbium-activated gadolinium oxysulfide plastic optical fiber sensor in photons and protons," *IEEE Sensors J.*, vol. 18, no. 4, pp. 1513–1519, Feb. 2018.

[11] F. Therriault-Proulx, L. Archambault, L. Beaulieu, and S. Beddar, "Development of a novel multi-point plastic scintillation detector with a single optical transmission line for radiation dose measurement," *Phys. Med. Biol.*, vol. 57, no. 21, pp. 7147–7159, Nov. 2012.

[12] M. Martyn, W. Kam, P. Woulfe, and S. O'Keeffe, "Water phantom characterization of a novel optical fiber sensor for LDR brachytherapy," *IEEE Sensors J.*, vol. 23, no. 2, pp. 1146–1156, Jan. 2023.

[13] S. Girard et al., "Gamma-rays and pulsed X-ray radiation responses of nitrogen-, germanium-doped and pure silica core optical fibers," *Nucl. Instrum. Methods Phys. Res. Sect. B, Beam Interact. Mater. At.*, vol. 215, nos. 1–2, pp. 187–195, Jan. 2004.

[14] S. Girard, J. Keurinck, Y. Ouerdane, J. P. Meunier, and A. Boukenter, "Γ-rays and pulsed X-ray radiation responses of germanosilicate single-mode optical fibers: Influence of cladding codopants," *J. Lightw. Technol.*, vol. 22, no. 8, pp. 1915–1922, Aug. 9, 2004.

[15] G. Origlio, M. Cannas, S. Girard, R. Boscaino, A. Boukenter, and Y. Ouerdane, "Influence of the drawing process on the defect generation in multistep-index germanium-doped optical fibers," *Opt. Lett.*, vol. 34, no. 15, p. 2282, 2009.

[16] K. Tanimura, C. Itoh, and N. Itoh, "Transient optical absorption and luminescence induced by band-to-band excitation in amorphous SiO_2," *J. Phys. C, Solid State Phys.*, vol. 21, no. 9, pp. 1869–1876, Mar. 1988.

[17] A. L. Tomashuk et al., "Enhanced radiation resistance of silica optical fibers fabricated in high O_2 excess conditions," *J. Lightw. Technol.*, vol. 32, no. 2, pp. 213–219, Jan. 15, 2014.

[18] B. Brichard, P. Borgermans, A. F. Fernandez, K. Lammens, and A. Decreton, "Radiation effect in silica optical fiber exposed to intense mixed neutron-gamma radiation field," *IEEE Trans. Nucl. Sci.*, vol. 48, no. 6, pp. 2069–2073, Dec. 2001.

[19] D. L. Griscom, "Fractal kinetics of radiation-induced point-defect formation and decay in amorphous insulators: Application to color centers in silica-based optical fibers," *Phys. Rev. B, Condens. Matter*, vol. 64, no. 17, pp. 1–14, Oct. 2001.

[20] S. Girard et al., "Combined high dose and temperature radiation effects on multimode silica-based optical fibers," *IEEE Trans. Nucl. Sci.*, vol. 60, no. 6, pp. 4305–4313, Dec. 2013.

[21] H. Henschel, O. Koehn, and H. U. Schmidt, "Influence of dose rate on radiation-induced loss in optical fibers," in *Proc. SPIE*, vol. 1399, Mar. 1991, pp. 49–63.

[22] D. L. Griscom, "Radiation hardening of pure-silica-core optical fibers: Reduction of induced absorption bands associated with self-trapped holes," *Appl. Phys. Lett.*, vol. 71, no. 2, pp. 175–177, Jul. 1997.

[23] H. Henschel and O. Kohn, "Regeneration of irradiated optical fibres by photobleaching?" *IEEE Trans. Nucl. Sci.*, vol. 47, no. 3, pp. 699–704, Jun. 2000.

[24] K. Nagasawa et al., "Improvement of radiation resistance of pure silica core fibers by hydrogen treatment," *Jpn. J. Appl. Phys.*, vol. 24, no. 9R, p. 1224, 1985, doi: 10.1143/JJAP.24.1224.

[25] S. Girard et al., "Recent advances in radiation-hardened fiber-based technologies for space applications," *J. Opt.*, vol. 20, no. 9, Sep. 2018, Art. no. 093001.

[26] P. Stajanca et al., "Effects of gamma radiation on perfluorinated polymer optical fibers," *Opt. Mater.*, vol. 58, pp. 226–233, Aug. 2016.

[27] O. J. Olusoji, W. Kam, and S. O. Keeffe, "Radiotherapy dosimetry based on perflourinated polymer optical fibres," in *Proc. SPIE*, vol. 353, 2020, Art. no. 113541W.

[28] O. J. Olusoji, C. Penner, C. Bélanger-Champagne, W. Kam, and C. Hoehr, "Proton Bragg peak detection with perfluorinated polymer fibre," in *Proc. OSA Opt. Sensors Sens. Congr.*, 2021, Art. no. STu4H.4.

[29] U. Schneider and R. Hälg, "The impact of neutrons in clinical proton therapy," *Frontiers Oncol.*, vol. 5, pp. 1–5, Oct. 2015.

[30] E. W. Blackmore, "Operation of the TRIUMF (20–500 MeV) proton irradiation facility," in *Proc. IEEE Radiation Effects Data Workshop Held Conjunct. IEEE Nucl. Space Radiat. Effects Conf.*, Jul. 2000, pp. 1–5.

[31] J. F. Ziegler, M. D. Ziegler, and J. P. Biersack, "SRIM—The stopping and range of ions in matter (2010)," *Nucl. Instrum. Methods Phys. Res. Sect. B, Beam Interact. Mater. At.*, vol. 268, nos. 11–12, pp. 1818–1823, Jun. 2010.

[32] S. Agostinelli et al., "GEANT4—A simulation toolkit," *Nucl. Instrum. Methods Phys. Res. Sect. A Accel. Spectrometers, Detect. Assoc. Equip.*, vol. 506, no. 3, pp. 250–303, 2003.

[33] E. W. Blackmore, P. E. Dodd, and M. R. Shaneyfelt, "Improved capabilities for proton and neutron irradiations at TRIUMF," in *Proc. IEEE Radiat. Effects Data Workshop*, Jan. 2003, pp. 149–155.

[34] S. Girard et al., "Overview of radiation induced point defects in silica-based optical fibers," *Rev. Phys.*, vol. 4, Nov. 2019, Art. no. 100032.

[35] P. Stajanca, L. Mihai, D. Sporea, D. Negut, and K. Krebber, "Perfluorinated polymer optical fiber for gamma radiation monitoring," in *Proc. 6th Eur. Work. Opt. Fibre Sensors*, vol. 9916, May 2016, Art. no. 99160H.

[36] K. Toh, K. Sakasai, T. Nakamura, K. Soyama, and T. Shikama, "Effects of neutrons and gamma-rays on polymethylmethacrylate plastic optical fiber," *J. Nucl. Mater.*, vol. 417, nos. 1–3, pp. 814–817, Oct. 2011.
[37] A. Leal-Junior et al., "Influence of gamma and electron radiation on perfluorinated optical fiber material composition," *Mater. Lett.*, vol. 340, Jun. 2023, Art. no. 134205.
[38] D. Sporea, L. Mihai, D. Neguţ, P. Stajanca, and K. Krebber, "Online monitoring of gamma irradiated perfluorinated polymer optical fiber," *Proc. SPIE*, vol. 9886, Apr. 2016, Art. no. 98861Q.
[39] P. Stajanca and K. Krebber, "Radiation-induced attenuation of perfluorinated polymer optical fibers for radiation monitoring," *Sensors*, vol. 17, no. 9, p. 1959, Aug. 2017.
[40] D. Di Francesca et al., "Distributed optical fiber radiation sensing in the proton synchrotron booster at CERN," *IEEE Trans. Nucl. Sci.*, vol. 65, no. 8, pp. 1639–1644, Aug. 2018.
[41] I. Toccafondo et al., "Distributed optical fiber radiation sensing in a mixed-field radiation environment at CERN," *J. Lightw. Technol.*, vol. 35, no. 16, pp. 3303–3310, Aug. 15, 2017.
[42] S. Girard et al., "Atmospheric neutron monitoring through optical fiber-based sensing," *Sensors*, vol. 20, no. 16, p. 4510, 2020.
[43] J. Niedermeier et al., "Optical fibers as dosimeter detectors for mixed proton/neutron fields—A biological dosimeter," *Electronics*, vol. 12, no. 2, pp. 1–12, 2023, doi: 10.3390/electronics12020324.

Olugbenga Jeremiah Olusoji (Member, IEEE) received the bachelor's and M.Sc. degrees in solid state physics from the University of Ibadan, Ibadan, Nigeria, in 2012 and 2015, respectively, and the master's degree in photonics from the Abbe School of Photonics, Friedrich Schiller University, Jena, Germany, in 2018. He is currently pursuing the Ph.D. degree with the Optical Fiber Sensors Research Center (OFSRC), Electronics and Computer Engineering Department, University of Limerick, Limerick, Ireland, working on the advancement of photonics in radiotherapy.

Crystal Penner (Member, IEEE) received the B.Sc. and B.Ed. degrees from the University of British Columbia, Vancouver, BC, Canada, in 2007 and 2009, respectively, and the M.Sc. degree in medical physics from the National University of Ireland, Galway, Ireland, in 2016. She is currently pursuing the Ph.D. degree in electrical and computer engineering with the University of British Columbia and TRIUMF, Vancouver.

Her work consists mainly of the fabrication and testing of scintillating and optical fiber sensors for proton, neutron, and photon dosimetry applications.

Camille Bélanger-Champagne (Member, IEEE) received the Ph.D. degree in physics from Uppsala University, Uppsala, Sweden, in 2011.

She is a Staff Scientist with TRIUMF, Vancouver, BC, Canada, where she coordinates the activities of the Proton and Neutron irradiation Facilities (PIF and NIF).

Vince Strgar received the B.A.Sc. degree in engineering physics from the University of British Columbia, Vancouver, BC, Canada, in 1994.

He currently performs QA and Commissioning of Medical Electron Accelerators with BC Cancer, Vancouver, as a Physics Assistant.

Eva Kasanda received the B.Sc. degree in biological and medical physics and the Ph.D. degree in nuclear physics from the University of Guelph, Guelph, ON, Canada, in 2017 and 2023, respectively.

She is currently a Postdoctoral Researcher with the Laboratory for High Energy Physics, University of Bern, Bern, Switzerland, working on medical applications of particle physics.

Cornelia Hoehr is the Deputy Director with the Life Sciences Division, TRIUMF, Vancouver, BC, Canada, where she is a Senior Research Scientist, and an Adjunct Professor with the University of Victoria, Victoria, BC, Canada, and the University of British Columbia—Okanagan, Kelowna, BC, Canada. Her research focuses on the targets for the production of novel medical isotopes and novel modalities for cancer therapy.

Sinead O'Keeffe (Member, IEEE) received the B.E. (Hons.) degree and the Ph.D. degree in electronic engineering from the University of Limerick, Limerick, Ireland, in 2003 and 2006, respectively.

She is a Royal Society–Science Foundation Ireland University Research Fellow with the University of Limerick. Her research focuses on optical fiber sensing for radiation dosimetry, primarily for radiotherapy applications.

Dr. O'Keeffe was a Member-at-Large of the IEEE Sensors Council for 2017–2020 and the Chair of the IEEE Sensors Council Diversity and Inclusion Committee (2020–2022).